Raman and infrared spectra of the incommensurate crystal Na$_2$CO$_3$

H. Meekes, Th. Rasing,* and P. Wyder[†]

Research Institute for Materials, University of Nijmegen, Toernooiveld, NL-6525 ED Nijmegen, The Netherlands

A. Janner and T. Janssen

Institute of Theoretical Physics, University of Nijmegen, Toernooiveld, NL-6525 ED Nijmegen, The Netherlands

(Received 15 August 1985)

The complete Raman spectra of Na$_2$CO$_3$ in its monoclinic (β), incommensurate (γ), and lock-in (δ) phases, as well as the far-infrared spectra in the γ and δ phases, have been measured and interpreted using symmetry and phenomenological arguments. Additional modes have been observed in the incommensurate phase as predicted by the superspace group selection rules of γ-Na$_2$CO$_3$. Two soft modes have been observed; one of them belongs to the monoclinic-to-incommensurate phase transition. Clear evidence has been found for the existence of a low-temperature commensurate (δ) phase.

I. INTRODUCTION

During the last ten years a growing interest in incommensurate crystal phases has developed. Besides structural investigations, a lot of work has been devoted to the study of lattice vibrations by means of light scattering. This paper is intended to give a contribution to this field by analyzing the Raman and infrared spectra of sodium carbonate (Na$_2$CO$_3$), which is a well-known example of a displacively incommensurate crystal structure. Some preliminary results herein have already been published elsewhere.[1]

Incommensurate modulated crystals are characterized by a periodic distortion (modulation) which in wavelength does not fit with the periodicities of the underlying undistorted lattice. Frequently, this crystal phase is intermediate between a high-temperature normal (N) phase and a low-temperature commensurate (C) phase, where the modulation wave vector is locked in to a rational value with respect to the reciprocal lattice of the undistorted crystal. The modulation can be of the displacive or of the density type, or of both.

One of the main consequences of the incommensurate nature of the modulation is the lack of lattice translational symmetry for this type of crystal. As many properties of normal crystals, such as the unit cell, Brillouin zone, phonons, etc., are closely related to the lattice translational symmetry, one could expect that all these properties will change drastically in the case of incommensurate structures. Experiment, however, shows that incommensurate crystals share most of the physical properties of the normal crystalline state. In particular, their diffraction patterns show the familiar sharp Bragg spots. A first description of the appearance of these crystalline properties can be found in the work of de Wolff[2] and Janner and Janssen.[3,4] In their approach, use is made of $(3 + d)$-dimensional space groups, so-called super-space groups. In the superspace the lattice symmetry of the incommensurate crystal is restored and one can again use notions such as Brillouin zone, Bragg plane, etc., but in more than three dimensions. The real crystal appears as an intersection with the three-dimensional space of a structure appropriately embedded in the superspace.

The use of space-group symmetry in deriving selection rules for light scattering is well established (see, e.g., Hayes and Loudon[5]). In the case of incommensurate structures the super-space groups play the role of space groups for normal crystals and corresponding selection rules are easily found. Moreover, the super-space groups can also be of help in the case of superstructures (e.g., commensurate crystal phases), even when the supercell is not a very large one.

The specific choice of sodium carbonate as a model structure for our experiments was made for two reasons. First of all, the structure of the crystal is known in its several phases and second, the modulation is quite significant, with amplitudes up to 0.4 Å. Both the modulation amplitudes and the wave vector are temperature dependent. Hence, the effects of the modulation on the phonon spectrum are expected to become apparent while going through the different phases of the crystal.

This expectation is also supported from the theoretical point of view. One knows that the behavior of excitations in the incommensurate phase depends on the super-space-group symmetry of the crystal. The selection rules for Raman and infrared (IR) active modes have already been shown to be relevant for the understanding of spectra of Rb$_2$ZnBr$_4$ (Rasing et al.[6]). Those for Na$_2$CO$_3$ will be derived further on.

The work done thus far on light scattering in the case of sodium carbonate has been limited to infrared transmission in the internal mode regime, and Raman scattering for two temperatures[7] and low-frequency Raman scattering for several temperatures.[8]

This paper is organized as follows. Section II deals with the structure of sodium carbonate. Experimental details and results are given in Sec. III. Section IV covers the interpretation of the results. Some conclusive remarks can be found in Sec. V.

II. THE STRUCTURE OF SODIUM CARBONATE

Sodium carbonate belongs to the A_2BX_n (with $n=3$ or 4) family of dielectrics, where several crystals are known to have an incommensurate modulated phase. In Na$_2$CO$_3$ there are at least three clearly distinguishable phases. Above 763 K a hexagonal structure (α phase) exists, stable up to the melting point at 1123 K. The structure in this phase has space group $P6_3/mmc$ (D_{6h}^4). Between 620 and 763 K the crystal is monoclinic (β phase) with space group $C2/m$. Below 620 K an incommensurate phase appears (γ phase). In addition, de Pater and Helmholdt[9] found in a neutron-diffraction experiment evidence for a fourth phase below 130 K (δ phase) in which the crystal is commensurate and forms a superstructure of the β phase.

The incommensurate (γ) phase has a one-dimensional modulation with wave vector $q=\alpha a^*+\gamma c^*$, where $\alpha=0.182$ and $\gamma=0.318$ at room temperature (b is the unique axis and c is the pseudohexagonal axis of the basis structure). In a harmonic approximation,[10] it has been found that the modulation is polarized along b for most of the atoms (with amplitudes up to 0.4 Å at room temperature), only two oxygen atoms of every CO$_3$ ion having a polarization with components along a and c too. The result is an overall displacive modulation along b, combined with a libration of the CO$_3$ ions in their plane and around the C—O direction perpendicular to b. The phases of the modulation wave are different for the various atoms in the unit cell of the basis structure. A projection of the C-centered cell and of the primitive cell in the β phase is given in Fig. 1. The atomic positions of the average structure at room temperature are the following:

Na(1)   : $r_1 = (0,0,0)$
Na(2)   : $r_2 = (0,0,\frac{1}{2})$
Na(3),C,O(2)   : $r_j = (x_j,\frac{1}{2},z_j)$ $(j=3,4,5)$
O(1),O(3)   : $r_j = (x_j,y_j,z_j)$ $(j=6,7)$

These positions are given with respect to the C-centered cell. The Na(1) and Na(2) atoms will be denoted as Na(I), when referred to in the α phase, because of their
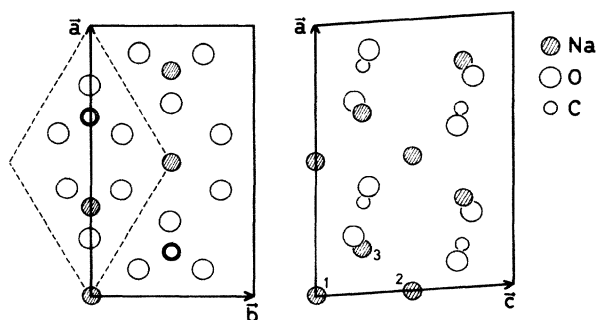

FIG. 1. Two projections of the C-centered cell of Na$_2$CO$_3$ in the monoclinic β phase. The primitive cell is drawn with broken lines in the projection along c. The numbers at the Na sites are referred to in the text. Note the pseudohexagonal symmetry.

equivalency in that phase. The generators of the point group $2/m$ (C_{2h}) are m_y: $(x,y,z)\rightarrow(x,\bar{y},z)$ and 2_y: $(x,y,z)\rightarrow(\bar{x},y,\bar{z})$. The Na and C atoms, as well as the O(2), are invariant under the mirror operation; the twofold axis leaves only Na(1) and Na(2) invariant.

The evidence for the presence of the δ phase was not very clear and not apparent in a number of subsequent experiments. We will come back to this question. According to de Pater[9] the commensurate value of the wave vector is $q=\frac{1}{6}a^*+\frac{1}{3}c^*$, leading to a twelvefold superstructure with respect to the β phase, with space group $P2/a$. (C_{2h}^4).

III. EXPERIMENTAL

A. Crystal preparation

The samples used in the unpolarized Raman and far-infrared (FIR) measurements have been cut from larger crystals grown by the Bridgman method. On going through the α-β transition the single crystals get microtwinned around the c^* axis with six possible domain orientations. Therefore, these crystals are not suitable for measurements using polarized light. The corresponding samples were opaque and roughly shaped. They were cut further and polished in order to improve the transparency of the faces. The final dimensions were approximately $4\times4\times4$ mm^3. All crystal manipulation was done in a dry nitrogen atmosphere to avoid hydration of the samples.

B. Raman measurements

The Raman measurements were made with an Ar$^+$-ion laser working at 514.5 nm as a source and a Spex Industries double-grating monochromator with spatial filter. Incoming and outgoing beams were mutually perpendicular. The photon counting has been done by standard equipment. The exciting continuous power used varied from approximately 0.03–1 W.

The complete unpolarized Raman spectra (internal and external modes) were measured from 40–685 K, with intervals of 20°. The spectral resolution was about 2 cm^{-1}. Frequency calibration was achieved by measuring the complete (attenuated) Rayleigh line for each spectrum. The error in the frequencies, however, is mainly due to the interpretation of the line form, and will depend strongly on temperature and specific mode (see below). Measurements above ~600 K were difficult or even impossible, because the samples tended to turn black at the spot where the laser light entered. By lowering the power of the laser radiation to 30 mW, the effect started at higher temperature. It is probably due to instability of the CO$_3$ ions under such conditions. The same phenomenon occurred, but then only above approximately 650 K, using a Nd-YAG laser working at 1064 nm in second harmonic generation experiments.[11] The surface of the sample was clearly destroyed by the radiation and the Raman signal disappeared. Hence, most of the measurements have been done in the γ and δ phases. A few examples of Raman spectra taken at various temperatures are presented in Fig. 2.
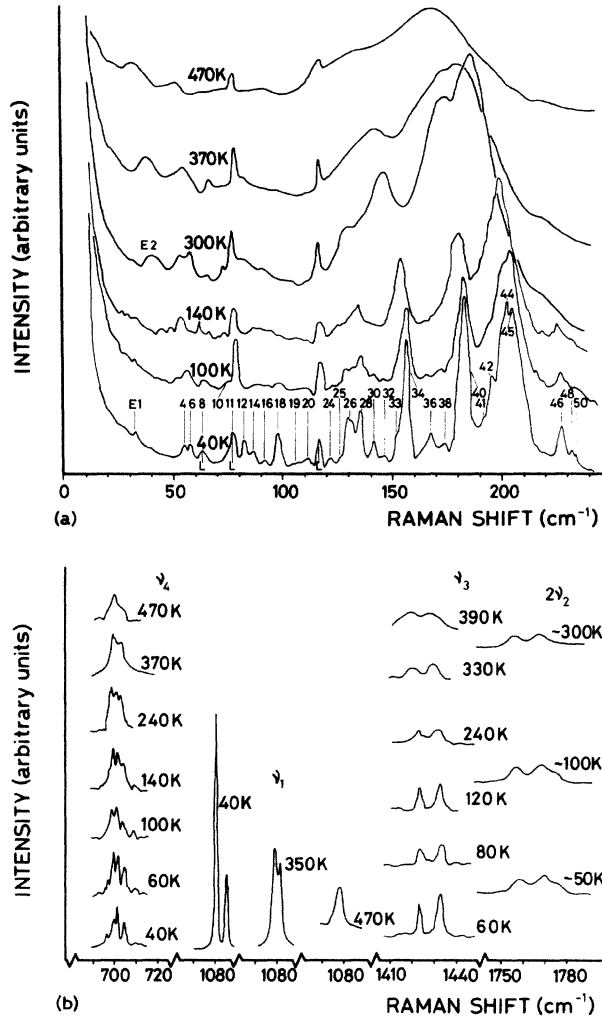
FIG. 2. Unpolarized Raman spectra of Na_2CO_3 for a few temperatures. Both the external (a) and internal (b) modes are drawn. The identifiers En and ν_n are referred to in the text; L indicates instrumental (laser plasma) lines.

FIG. 3. Raman shift versus temperature for the external modes (a) and the internal modes (b) of Na_2CO_3. Indicated are the lock-in transition temperature (T_c) and the incommensurate phase-transition temperature (T_i). The identifiers En are given for the most significant lines. The squares, circles, and diamonds refer to different samples used and do *not* indicate the experimental error. The two highest-internal-mode data (full circles) are from earlier measurements, using 1-W laser power.

With an exception for two soft modes, the instrumental line shape was not deconvoluted, nor fitted to a Lorentzian because we consider this inadequate for complex incommensurate structures like Na_2CO_3. The line form of a mode in the incommensurate phase is made up of many individual lines, whose mutual intensity ratios depend strongly on temperature as will become clear in Sec. IV E. Because of this and the large number of phonon branches in Na_2CO_3 one would need too many parameters in a fit to be valuable. More simple (well-known) incommensurate structures could be appropriate for such an analysis. Therefore, we have measured the frequency by taking the middle of the upper peak part of a line, assuming that the $k=0$ contribution is the largest and manifests itself as such a peak, for temperatures not too close to the lock-in transition. Furthermore, we are not interested in the exact phonon frequencies but rather in the global temperature dependence and splitting of lines. The frequency shifts as
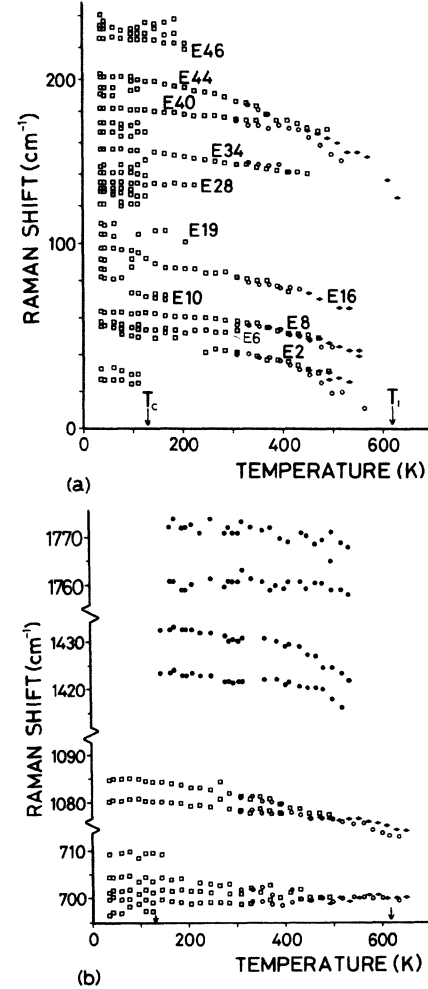
a function of temperature are plotted for all Raman lines in Fig. 3.

In the case of the soft modes, which will be treated in Sec. IV C, the peak frequencies (ω_p) were obtained by substracting the Rayleigh wing. The mode frequencies (ω_0) were calculated with $\omega_0^2 = \omega_p^2 + \frac{1}{2}\Gamma^2$, where Γ is the full width at half maximum of the Raman line. This expression follows when the mode is interpreted as a damped harmonic oscillator, whose Raman intensity is given by

$$I(\omega,T) = K\frac{[n(\omega,T)+1]\omega\Gamma\omega_0^2}{(\omega_0^2 - \omega^2)^2 + \omega^2\Gamma^2} \qquad (1)$$

(see, e.g., Hayes and Loudon;[5] K is a constant with respect to ω and T) and the Bose-Einstein factor (n) is approximated by $kT/\hbar\omega$ (for $T \approx 500$ K and $\omega \approx 30$ cm^{-1}).
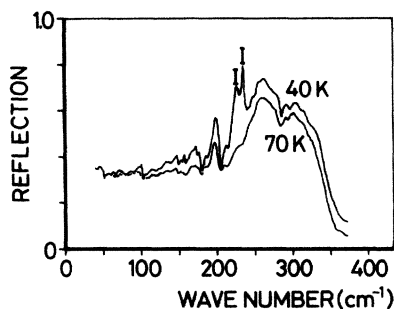
FIG. 4. Far-infrared reflection spectrum of the external modes of Na$_2$CO$_3$ for two temperatures. I denotes two instrumental peaks.

C. FIR measurements

The FIR experiment consisted mainly of reflection measurements at 45° for the incoming and outgoing light. A Michelson interferometer has been used as a FIR source. The detector consisted of either a He-cooled bolometer or a Golay cell.

The FIR reflection spectra were measured from 40—375 K. For higher temperatures the lines grew too broad to give any new information. Two spectra are presented in Fig. 4. The internal modes were not measured. For the lowest wave numbers (up to 60 cm^{-1}) some transmission data were available.[12] No measurements were done in the α and β phases.

D. Temperature control

The samples were mounted in a He gas-flow cryostat for temperatures from 4—300 K. For temperatures from 300—700 K the samples were heated in the same "cryostat." Special care was taken to be sure of the sample temperature, as will be explained below. Owing to both the very low and very high temperatures used in the Raman measurements, the crystal (mounted on a cold/hot finger) showed a very large temperature gradient over the sample in the earlier measurements. On the other hand, the crystal seemed to be quite absorbing for the laser light used. Therefore, a pyrex cell was constructed, which was filled with He exchange gas. The cell was shielded (except for holes for the ingoing and outgoing light) by a copper radiation shield at about the same temperature as the sample. A second copper radiation shield was placed within the outer cryostat case. The laser output power was kept smaller than 0.2 W, for which no influence on the spectra

TABLE I. The number of Raman and IR active vibrational modes of the free CO$_3$ ion. The corresponding symmetries in the α and β phases of Na$_2$CO$_3$ are indicated.

$\overline{6}m2$ (D_{3h})	n(vibr)	Activity	α-Na$_2$CO$_3$	β-Na$_2$CO$_3$
A_1'	1	Raman	$A_{1g}+B_{2u}$	A_g+B_u
A_2''	1	IR	$B_{1g}+A_{2u}$	A_g+B_u
E'	2	Raman	$2E_{2g}$	$2A_g+2B_g$
		IR	$2E_{1u}$	$2A_u+2B_u$

was observed. All results given were measured with this arrangement, unless otherwise specified.

The temperature of the sample was measured within the copper cold/hot finger just above the crystal, by means of a chromel-constantan thermocouple. This finger served also as a source for the temperature of the contact gas. Especially at the lowest (40 K) and highest (650 K) temperatures, this resulted in reliable measurements. For the FIR measurements the sample was almost completely enclosed by a copper block. The temperature has been measured at the crystal's backside with a chromel-constantan thermocouple. We estimate the absolute error in the temperatures to be less than 5°; the relative error probably less, both for the Raman and FIR measurements.

IV. INTERPRETATION

Owing to the lack of single crystals and the large number of Raman and FIR active normal modes in Na$_2$CO$_3$ the assignment of the lines observed is rather difficult. A great deal, however, can be done on the basis of the selection rules one has for the different phases and, of course, the analysis of the influence of the modulation on the different modes. Combining these elements in a consistent way, we were able to reach a fairly complete understanding of all the spectra. Occasionally we compare the results with those already published on K$_2$CO$_3$ and Rb$_2$CO$_3$ (Brooker and Bates[13]), because these structures (though commensurate) show a great resemblance to sodium carbonate.[14] We will start with a derivation of the selection rules for light scattering in the different phases.

A. Optical activity of the modes

The optical activity of modes at $\mathbf{k}=0$ in the α and the β phases has been obtained by standard methods based on space-group symmetry whereas that of the modes in the γ phase was obtained correspondingly by using super-

TABLE II. The number of Raman and IR active modes in the α phase of Na$_2$CO$_3$. Parentheses indicate the acoustical modes which are not active.

$6/mmm$ (D_{6h})	n(acoust)	n(opt tr)	n(rot)	n(vibr)	Activity
A_{1g}	0	0	0	1	Raman
E_{1g}	0	0	1	0	Raman
E_{2g}	0	2	0	2	Raman
A_{2u}	(1)	2	0	1	IR
E_{1u}	(1)	2	0	2	IR

TABLE III. The Raman and IR active modes in the β phase of Na_2CO_3. Parentheses indicate the acoustical modes which are not active.

$2/m$ (C_{2h})	n(acoust)	n(opt tr)	n(rot)	n(vibr)	Activity
A_g	0	4	1	4	Raman
B_g	0	2	2	2	Raman
A_u	(1)	3	2	2	IR
B_u	(2)	6	1	4	IR

space-group methods. For a review on the use of space-group symmetry in deriving selection rules for light scattering (Raman and IR) see, e.g., Hayes and Loudon.[5]

One distinguishes between internal modes (relative vibrations of CO_3 constituents) and external modes (the remaining lattice vibrations). The latter have been considered in the rigid-ion approximation, where the CO_3 ion is considered as a rigid molecule because of the much stronger bonds within the ion as compared to the "external" lattice bonds. Next to the internal modes, one then gets a number of librational (CO_3 ion), optical, and acoustical translational modes that transform according to irreducible representations of the corresponding space group. We will use the Mulliken notation for these irreducible representations. The number of vibrational modes of the free CO_3 ion (symmetry group D_{3h}) and their symmetry are given in Table I. The results for the α phase of Na_2CO_3 are summarized in Table II, those for the β phase are given in Table III.

The optical activity of fundamentals is for normal crystals restricted to modes at $k=0$. In the case of incommensurate crystals, however, the modes at $k=n\mathbf{q}$ (where $\mathbf{q}$ is the incommensurate wave vector and n an integer) are equivalent to those at $k=0$ (Janssen[15]). Therefore, modes at $k=n\mathbf{q}$ may become optically active, depending on the symmetry with respect to the point group. The modes can be labeled by the irreducible representations of the three-dimensional point group isomorphic to that of the super-space group. In the case of Na_2CO_3 the super-space-group is $P^{C2/m}_{\bar{1}\ s}$ (Janner and Janssen[3]), and the point group is thus isomorphic to $2/m$. With the help of the super-space-group the symmetry of modes at $k=n\mathbf{q}$ can be derived. Because the intensity of modes in a light-scattering experiment is expected to decrease very fast with growing n in the case of a sinusoidal modulation,[16,17] the selection rules are derived only for $n=0,\pm1$. The results are given in Table IV. The details of the change in selection rules due to the transition to the δ phase will be given later.

The basis vectors of the irreducible representations containing one or more phonon modes, have been derived in all the phases. They were not strictly determined by the representations of the β phase; the eigenvector is assumed to differ not much from that of the corresponding mode in the α phase. The results for the external modes in the α and β phases are given in Table V.

B. The internal modes

As already was pointed out, a distinction has to be made between internal and external modes. The internal modes describe vibrations inside the CO_3 ion, which has very strong bonds. Accordingly, its vibrational modes occur at rather high frequencies. For Na_2CO_3, external modes typically have frequencies ω below 350 cm^{-1}, whereas the internal modes lie near 700, 880, 1080, and 1420 cm^{-1}, respectively. Owing to these high frequencies, the coupling of the internal modes to the lattice is small. The dispersion of the internal modes is therefore very flat. Furthermore, comparing the values of the vibrational modes of the free CO_3 ion[18] with those in the crystal, one finds a difference in frequency of about 3, 0, 2, and 5 % respectively. Hence, the internal modes can be treated, within a good approximation, as local modes; the frequency being determined by the structure of the CO_3 ion itself and by the local surrounding of that ion. This local character is expected to be more pronounced the higher the frequency. The external modes must be treated, of course, as ordinary phonon modes, which extend (in principle) through the whole crystal.

Owing to the flat dispersion of the internal modes, the presence of a displacive modulation gives rise to a modulated shift in frequency for the individual ions with respect to that of an average structure. Therefore, the experimental line shape of the internal modes in the incommensurate phase shows a frequency distribution reflecting properties of the modulation. Which type of distribution one has to consider in the case of sodium carbonate was

TABLE IV. The Raman and IR active modes in the γ phase of soda, indicated as $n_{k=0}+n_{k=\pm q}$. Parentheses indicate the acoustical modes which are not active.

$2/m$ (C_{2h})	n(acoust)	n(opt tr)	n(rot)	n (vibr)	Activity
A_g	$0+1$	$4+5$	$1+4$	$4+4$	Raman
B_g	$0+2$	$2+10$	$2+2$	$2+8$	Raman
A_u	$(1)+2$	$3+10$	$2+2$	$2+8$	IR
B_u	$(2)+1$	$6+5$	$1+4$	$4+4$	IR

suggested by de Wolff and Tuinstra[14] on the basis of a model developed by Blinc *et al.*[19] for NMR measurements. We will call it the de Wolff-Tuinstra-Blinc (WTB)-model and use it, taking into account the case of an incommensurate modulation involving more than one harmonic.

On going through the crystal, the local field felt by the CO_3 ion takes all values between zero and the one due to a maximum displacement. We expand the frequency of an internal mode of the CO_3 ion in a power series of the order parameter η, which describes the local effect of the modulation:

$$v=v_0+a_1\eta+\frac{a_2}{2}\eta^2+\cdots . \qquad (2)$$

In Eq. (2) only even powers in η contribute, due to the $\binom{m}{s}$ symmetry element of sodium carbonate. The frequency distribution $f(v)$ depends on the density of ion sites $\rho_j(r)$

according to

$$f(v)dv=\rho(\xi)d\xi ,$$

or

$$f(v)=\frac{\rho}{|\nabla v|} , \qquad (3)$$

where $\xi \equiv q \cdot r$. In the case of sodium carbonate one knows that higher harmonics in the modulation wave have a nonnegligible effect and become very important near the lock-in transition. Accordingly we write for the order parameter

$$\eta= \sum_{n=1}^{N} f_n\sin(nq \cdot r+\phi) , \qquad (4)$$

where we assume that all harmonics are in phase. From Eq. (3) follows that $f(v)$ and hence the intensity of the signal in the light scattering experiment diverge when

TABLE V. Basis vectors of the external modes transforming corresponding to the different irreducible representations in the α and the β phase. Note that the acoustical modes are also present among the translational modes. Symm. and a-symm. means symmetric and antisymmetric, respectively, under a permutation of two equivalent ions; Na(I) stands for Na(1) or Na(2). The numbers are referred to in the text. A justification of the assignment to the Raman lines (at $k=0$) and the clusters (Cn) in the δ phase can be found in Secs. IV C, IV D, and IV F; for the clusters see also Table VII.

α phase	β phase	Mode		Number	Assignment
		Acoustical			
A_{2u}	B_u	along c		1	
E_{1u}	A_u	along b		2	
	B_u	along a		3	
		Librational			
A_{2g}	B_g	CO_3 around c	symm.	4	$E16$ ($C16$)
E_{1g}	A_g	CO_3 around b	symm.	5	$E8$ ($C8$)
	B_g	CO_3 around a	symm.	6	In Rayleigh line ($E2$ at $k=\pm q$)
B_{2u}	A_u	CO_3 around c	a-symm.	7	
E_{2u}	A_u	CO_3 around a	a-symm.	8	
	B_u	CO_3 around b	a-symm.	9	
		Translational			
B_{2g}	A_g	CO_3 along c	a-symm.	10	Mainly $E10$ ($C10$)
		Na(3) along c	a-symm.	11	Mainly $E19$ ($C19$)
E_{2g}	A_g	CO_3 along a	a-symm.	12	Mainly $E34$ ($C34$)
		Na(3) along a	a-symm.	13	Mainly $E40$ ($C40$)
	B_g	CO_3 along b	a-symm.	14	Mainly $E28$ ($C28$)
		Na(3) along b	a-symm.	15	Mainly $E44$ ($C44$)
A_{2u}	B_u	CO_3 along c	symm.	16	
		Na(3) along c	symm.	17	
		Na(I) along c	symm.	18	
B_{1u}	B_u	Na(I) along c	a-symm.	19	
E_{1u}	A_u	CO_3 along b	symm.	20	
		Na(3) along b	symm.	21	
		Na(I) along b	symm.	22	($C48$)
	B_u	CO_3 along a	symm.	23	
		Na(3) along a	symm.	24	
		Na(I) along a	symm.	25	
E_{2u}	A_u	Na(I) along b	a-symm.	26	
	B_u	Na(I) along a	a-symm.	27	

$|\nabla v|=0$; hence, i.e., when $\eta=\eta_{min}=0$ or $\eta=\pm\eta_{max}$. This means that the line shape of the internal modes shows two edge singularities, independent of the number of harmonics involved. The intensity ratio of both singularities however, depends on the number of those harmonics. For a single harmonic modulation [$N=1$ in Eq. (4)], the intensity due to the two singularities will be equal. This is expected to be the case just below the incommensurate phase transition. For temperatures in the neighborhood of the lock-in transition, the number of relevant harmonics in the modulation increases rapidly (discommensuration regime) and the modulation waveform is rather squarelike than sinusoidal. In this regime the intensity of the line at the singularity point corresponding to $\eta=\pm\eta_{max}$ will be stronger than that at the $\eta=0$ singularity point. A more quantitative approach is only possible if one knows the form of the modulation wave. In the commensurate phase the line form may change due to the commensurate value of the modulation wave vector.

In what follows, each internal mode is discussed in some detail. The experimental data used are taken from Brooker and Bates[7,13] for material relevant to the IR internal modes of Na_2CO_3 and the IR and Raman data of K_2CO_3 and Rb_2CO_3, whereas the Raman data on Na_2CO_3 are based on our own measurements. Symmetry considerations are given here for the β phase; the reader is reminded that the γ phase is a modulated β-phase structure and that all measurements have been collected in either the γ or the δ phase. For the experimental results see Figs. 2 and 3.

1. The v_1 internal mode

This is the totally symmetric breathing mode, with free-ion frequency 1063 cm^{-1}, symmetry A'_1 (Raman active only), giving rise to an A_g and a B_u symmetry mode in the crystal field of the β phase. The IR active B_u component is not observed, while the A_g component is very strong in the Raman spectrum. The observed Raman signal consists of two sharp peaks at approximately 1080 and 1085 cm^{-1}, respectively, at the lowest temperature. Hence, the observations fit well with the WTB model. The intensity ratio of the two peaks and the frequency difference of both plotted versus temperature are given in Fig. 5. If we extrapolate the intensity ratio linearly to the value 1, we find a temperature of approximately 560 K, interpreted as the temperature above which the modulation is mainly sinusoidal. For lower temperatures, the low-frequency component becomes the strongest and this line can therefore be interpreted as corresponding to the $\eta=\pm\eta_{max}$ singularity. Below 140 K (which is just above the lock-in transition at 130 K) the ratio is 0.2 to 0.4.

In the model, the frequency difference between the two discontinuities is given by $\frac{1}{2}a_2\eta_{max}^2$ and therefore it depends on the amplitude and number of higher harmonics of the modulation. Experimentally, below ~140 K, this difference is almost constant indicating that the waveform is fairly stable below T_c. Above that temperature range the frequency difference decreases linearly until about 310 K, where it drops to a lower value. For temperatures above approximately 390 K the difference is too small to
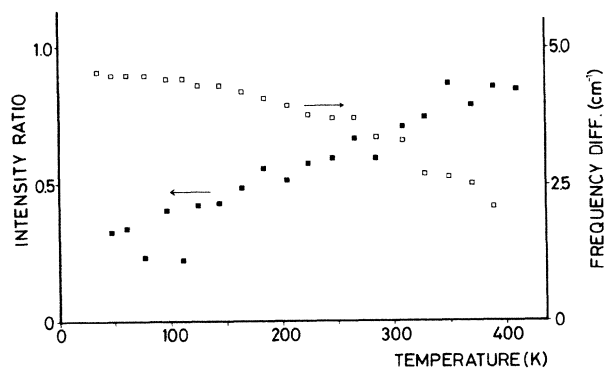

FIG. 5. Frequency difference and peak-intensity ratio of the two components of the v_1 internal mode of Na_2CO_3 versus temperature. The squares do *not* give the experimental error.

be detected. The step behavior at 310 K could be related to the fact that the wave vector of the modulation locks in to a value lying on the line $\alpha+\gamma=\frac{1}{2}$ below 300 K, with only quite small changes in its absolute value.[9] An extrapolation to zero splitting would be tentative. In the case of K_2CO_3 and Rb_2CO_3 the IR component was very weak and this is consistent with the idea of a small influence of the lattice.

2. The v_2 internal mode

The free-ion frequency of this mode is 879 cm^{-1}, its symmetry A''_2, and it is IR active. It consists of polar movements perpendicular to the plane of the ion. Under influence of the crystal field of the β phase this mode splits into two components, A_g+B_u; hence, Raman and IR active, respectively. The Raman active component however, was not observable, the IR component being quite strong, which is a further indication for the weak coupling between the ions. However, a two-phonon v_2 Raman component was seen, although very weak. The selection rules for such a two-phonon process imply

$$\Gamma(\text{two-phonon } v_2)=2A_g+2B_u \ , \tag{5}$$

where $A_g\times A_g=B_u\times B_u=A_g$ and $A_g\times B_u=B_u$; hence, three different lines are expected.

In the IR, one line is expected in the β phase. In the γ phase the spectrum consists of two lines at 880 and 886 cm^{-1}, respectively, which again fits well in the WTB model. When using high-exciting powers up to 1 W, three Raman lines were resolved below approximately 140 K (N.B., these temperatures are not reliable due to heating of the sample by the high power of the laser used and the bad cooling during that measurement). The corresponding frequencies were observed at 1758, 1770, and 1775 cm^{-1}. At higher temperatures and in later measurements only two lines were seen at 1760 and 1772 cm^{-1}. The last two are exactly twice the value of the IR data and are therefore expected to be of the type $B_u\times B_u$. The $A_g\times A_g$ component is probably too weak, but could have given rise to the 1775-cm^{-1} line of the early measurements. The

splitting of the two Raman lines seems to be constant up to approximately 450 K, although the intensity is too weak to draw definite conclusions. A striking feature, however, is the fact that the intensity of the 886-cm^{-1} IR line is smaller than that of the 880-cm^{-1} line at 300 K, while the two two-v_2 intensities are comparable. This difference could be due to the less stringent demands on the phonon wave vectors for a two-phonon process ($q_1+q_2=0$), which also explains the broader Raman lines as compared to the IR fundamentals. In the case of K_2CO_3 and Rb_2CO_3 also, the Raman v_2 line was not observable, while the two-v_2 component was present, although a few cm^{-1} higher than twice the fundamental frequency.

3. The v_3 internal mode

The v_3 mode is a doubly degenerate E' mode (Raman and IR active) with frequency 1415 cm^{-1}, consisting of nonsymmetric motions in the plane of the ion. In the crystal field these modes split according to $A_g+B_g+A_u+B_u$, which are Raman and/or IR active. Because the unperturbed free-ion modes are already active, one expects that the perturbed crystalline modes are also observable in both the Raman and IR spectra. This is indeed the case. The IR spectrum consists of two lines at 1413 and 1425 cm^{-1} and the Raman spectrum also of two lines at 1422 and 1431 cm^{-1}. The splitting is probably due to the crystalline field, which is also supported by the temperature dependence of the frequency difference of the two components. The movements of the O atoms are much smaller than those of the C atom. This mode, therefore, is less perturbed by the surrounding ions, than in the case of the v_1 and v_2 modes. Hence, the value of a_2 in Eq. (2) is much smaller for the v_3 mode than for the v_1 and v_2 ones and the two singularities are probably not resolved. A third small peak is observed at about 1450 cm^{-1}, when using high-exciting power (≈ 1 W). In such a situation this peak shows the same frequency dependence with temperature as the first two up to 300 K, where its frequency is 1448 cm^{-1}. In measurements done at less power, it is no longer observed. The Raman spectra of Brooker and Bates[7] show the same peak at 1448 cm^{-1} (at room temperature), but the authors do not mention it. The frequency difference between this line and the first two, makes an assignment to a v_3 mode rather difficult. In the case of K_2CO_3 and Rb_2CO_3 all Raman components were resolved, but the IR lines were broad and not all resolved.

4. The v_4 internal mode

This mode is also a doubly degenerate E' mode with frequency 680 cm^{-1}. It consists of nonsymmetric movements in the plane of the ion, the C atom having the largest amplitude. In the IR three components were seen at 694, 701, and a very weak line at 706 cm^{-1}. Brooker and Bates[7] found only two Raman components, while we observe three lines resolved below 300 K. Below T_c five modes can be seen. The A_g and B_u components consist of motions along a, while the B_g and A_u components have

motions mainly along b. The modulation has displacements along b mainly; hence, one expects the splitting of the two singularities to be the strongest for the B_g and A_u components, as compared with the other ones. This can explain the three observed modes in the IR and Raman spectrum. On the other hand it is possible that the edge singularities of the different v_4 components are not resolved. This would be the case if the splitting of the low-frequency component is the same as (or somewhat less than) that of the high-frequency component. The fact that for this internal mode more lines are resolved on going from the γ to the δ phase, is probably due to a larger dispersion as compared to the other internal modes which have a higher frequency or higher symmetry. We will come back to this subject, when we treat the lock-in transition. In the case of K_2CO_3 and Rb_2CO_3 all Raman components and three of the four IR lines were observed.

C. The soft modes

Before turning our attention to the external mode spectra we would like to discuss the soft modes which play an important role in the α-β and the β-γ phase transitions. As in Na_2CO_3, several phase transitions are driven by soft phonons; the question arises whether they are visible in the spectra. The various soft modes responsible for the different phase transitions have been found theoretically by Maciel and Ryan[8,20] and de Wolff and Tuinstra.[14] Let us mention them in order to get an overall picture.

At the hexagonal-to-monoclinic phase-transition temperature (T_α), the doubly degenerate symmetric librational mode of the CO_3 ions becomes soft. Below T_α this mode becomes hard and splits up in the a and b polarized components. These components are both Raman active. The E symmetry acoustic mode at $(0,0,q_3)\approx 0$ couples to the E_{1g} mode but is of course not visible in the spectra.

At the monoclinic-to-incommensurate phase-transition temperature T_i the symmetric librational mode around the a axis becomes soft together with the b polarized acoustic mode, both at $k=\pm q$, being not Raman active, nor IR active above the transition temperature. Below T_i the librational mode hardens giving rise to Raman and IR active components at $k=\pm nq$. The acoustic mode splits into an amplitudon which grows hard and a phason at zero frequency, the amplitudon being Raman active. Below the lock-in transition at T_c, the original phason mode grows hard, resulting in an IR active mode at nonzero frequency.

Maciel and Ryan[8] have looked at the low-frequency Raman spectrum and have found two "hard" modes which they ascribed to the two librational modes belonging to the hexagonal phase transition. They compared their results with measurements on K_2CO_3, where only one mode for the hexagonal phase transition was found.[20] Their explanation was that in K_2CO_3 the component of the soft mode that did not induce the transition to the monoclinic phase, stayed low in frequency, hidden under the Rayleigh line. The observation of this mode in Na_2CO_3 was explained to be due to a larger anisotropy in the hexagonal plane.

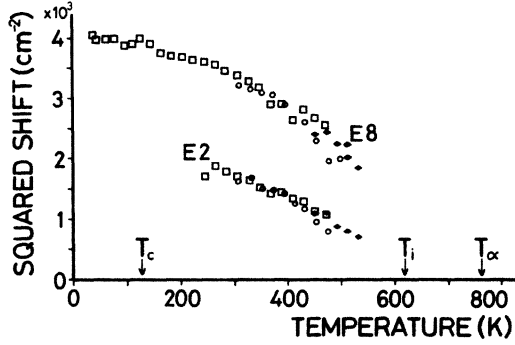We found the same modes, however, with different

FIG. 6. Squared frequency shift versus temperature for the two soft modes ($E8$ and $E2$) of Na_2CO_3. Indicated are the hexagonal-to-monoclinic phase-transition temperature (T_α) and the incommensurate phase-transition one (T_i). Again three different samples have been used; the experimental error is *not* indicated.

behavior as a function of temperature. In fact, in our case, the highest mode ($E8$) extrapolates to zero at T_α, but the lowest one ($E2$) does not (Figs. 6 and 3). If we extrapolate the mode frequency (ω_0, see Sec. III B) to zero, we find a temperature between T_α and T_i. We are very certain of the temperature values obtained in our measurements, because as mentioned in Sec. III, we paid much attention to this point. It is, however, difficult to find an exact extrapolation, due to the scattering of data points. nevertheless, the data tend more towards T_i then to T_α.

Moreover, we think that also in Na_2CO_3 one of the two librational modes stays at low frequency (B_g). This conclusion has been obtained on the basis of the same model as used by Maciel and Ryan. In that model the Landau free energy is written as a power series of the order parameter ϕ (given by the tilt angle of the CO_3 ions), up to sixth order:

$$F = \frac{1}{2}\alpha(T)\phi^2 + \frac{1}{4}V\phi^4 + \frac{1}{6}W_1\phi^6(\eta_1^6 + 9\eta_1^2\eta_2^4 - 6\eta_1^4\eta_2^2)$$
$$+ \frac{1}{6}W_2\phi^6(\eta_2^6 + 9\eta_2^2\eta_1^4 - 6\eta_2^4\eta_1^2) + \frac{1}{4}C_{44}(e_4^2 + e_5^2)$$
$$+ g\phi(e_4\eta_1 + e_5\eta_2) . \tag{6}$$

The η_i are the coordinates of the librational mode with $\eta_1^2 + \eta_2^2 = 1$; $\alpha(T) = A(T - T_0)$. Terms representing elastic strains and a linear coupling of the order parameter to shear strains is included. Minimizing the free energy with respect to the order parameter one finds

$$\phi^2 = \frac{1}{2W_1}\{-V \pm [V^2 - 4W_1\alpha'(T)]^{1/2}\} , \tag{7}$$

where $\alpha'(T) = A(T - T_c)$ and $T_c = T_0 + 2g^2/(AC_{44})$. In the case of a first-order phase transition, the order parameter will have a spontaneous nonzero value at the transition temperature. In the case of sodium carbonate, the tilt angle of the CO_3 ions is linearly related to the angle β of the monoclinic cell. This appears very clearly in the mechanical model of de Wolff and Tuinstra.[14] The angle β has been measured as a function of temperature by Crooijmans[21] and shows a quadratic behavior in the neighborhood of the transition

$$\left[\frac{\beta(T) - 90°}{360°}\right]^2 = A'(T - T_\alpha) \tag{8}$$

above approximately 690 K, with $A' \approx 4.7 \times 10^{-6}$ K^{-1}. Such a behavior is expected in the case of a second-order transition. Therefore, we conclude that indeed the transition is of second order (cf. de Pater and Helmholdt[9]). This implies that $T_\alpha \approx T_c$, $V > 0$, and $W \ll V$. The order parameter becomes simply

$$\phi^2 \approx -\frac{A}{V}(T - T_c) . \tag{9}$$

The frequencies ω_i of both librational components can be expressed as

$$\omega_1^2 \approx -2A(T - T_0) + \frac{2g^2}{C_{44}}$$

and $\tag{10}$

$$\omega_2^2 \approx \frac{2g^2}{C_{44}} .$$

If we use our data for $\omega_1^2(T)$ we find an upper limit of 14 cm^{-1} for ω_2 in the worst case of extrapolation. Even if we use the data of Maciel and Ryan this becomes $\omega_2 \approx 19$ cm^{-1} as upper limit. Both these values are smaller than the frequency of the lowest-lying soft mode ($E2$) and actually lie in the Rayleigh wing. Therefore, we conclude that this mode does not indeed belong to the hexagonal, but to the incommensurate phase transition, and is probably the mode corresponding to the soft librational phonon at $k = \pm q$. This conclusion is supported by the fact that the acoustic E_1 symmetry branch, which couples to the soft mode for the hexagonal phase transition, also has one component which stays low in frequency throughout the β phase. This follows from diffuse scattering observed in x ray and neutron-diffraction experiments.[14] The amplitudon probably lies at lower frequency than the above-mentioned mode, as it originates from an acoustic branch at $k = \pm q$. In K_2SeO_4, e.g., it lies at approximately 35 cm^{-1} (Wada et al.[22]). Hence, we expect this mode to be somewhere close to the Rayleigh line, as mentioned before. Maciel and Ryan found a mode at approximately 35 cm^{-1}, which they ascribed to the amplitudon.

A fourth Raman line was found at low temperatures, somewhere between the two soft modes and interpreted as the $k = \pm q$ mode, belonging to the lowest soft mode. The same mode was found by the authors: $E6$ in Figs. 2 and 3. Looking at its temperature dependence we would rather suggest that this mode is the $k = \pm q$ component of the upper soft mode. At the lowest frequencies (below about 30 cm^{-1}) some structure was observed in the tail of the Rayleigh line, especially when using high-exciting power. This structure does not reproduce well for different temperatures. This can be explained by the presence of $k = \pm nq$ components of the acoustic modes, which overlap and which change in frequency and intensity as a function of a varying form of the modulation wave and its wave vector. We will now discuss the remainder of the external mode spectra.

D. The external modes in the γ phase

In this section we devote our attention to the interpretation of the external mode spectra in the γ phase.

1. The Raman spectra

As one sees immediately (Figs. 2 and 3), the number of lines is too big to make the standard method for assignment useful. At the lowest temperature there are about 30 resolved lines, which have been numbered up to 50 (see Fig. 2). At higher temperatures these lines cluster together giving rise to about 11 lines just below 200 K. We will start with the interpretation of these 11 lines ($E46$, $E44$, $E40$, $E34$, $E28$, $E19$, $E16$, $E10$, $E8$, $E6$, and $E2$).

The selection rules for the β phase give at most nine observable lines, three rotational and six translational modes. Hence, there is at least one additional mode, which is specific for the incommensurate γ phase. Indeed only the average structure of the γ phase has the same space-group symmetry as the β phase. We can furthermore consider the gross structure of the spectrum due to the average structure as a slightly deformed high-temperature α phase. We thus make use of the selection rules valid in the α phase. In this phase all modes of symmetry A_{2g}, B_{2u}, E_{2u}, B_{2g}, B_{1u}, and E_{2u} are not active in the Raman, nor in the IR spectra. At the phase transition from the hexagonal-to-monoclinic phase all these modes become active (A_g, B_g, A_u, or B_u) in principle. The modes which

are not active in the α phase are expected to have a low intensity in the β-phase spectra, as compared to the modes which are active in both phases. These weak Raman active modes are numbers 4, 10, and 11 in Table V. The modes which are expected to be strong in the β phase are numbers 5, 6, 12, 13, 14, and 15 in Table V. Two of these last six modes are the soft modes of the α-β or β-γ transition, grown "hard." These give rise to the lines $E8$ and $E2$, and have already been treated, together with $E6$, in the section concerning the soft modes. It remains to discover four strong modes in the Raman spectrum. In Fig. 2 we indeed see four strong modes, namely $E44$, $E40$, $E34$, and $E28$. In this figure we also observe (cf. Fig. 3) that $E44$ and $E40$ grow towards each other at higher temperatures. The same holds for $E34$ and $E28$. This decreasing splitting is related to the angle β approaching 90° when the temperature comes close to 763 K. Therefore we expect both the $E40$-$E44$ and the $E28$-$E34$ pairs to be degenerate in the α phase. Because of the higher mass of the CO_3 ion with respect to that of Na [$M(CO_3) \approx 2.6M(Na)$] the low-frequency modes ($E28$-$E34$) will correspond to normal modes for which mainly the CO_3 ions move, either along **a** or **b**, while the pair $E40$-$E44$ corresponds to a similar mode, consisting primarily of Na(3) motions. Because the modulation is mainly polarized along **b**, one expects that the modes which at the lowest temperature consist of many resolved lines correspond to motions along **b** (see also the section devoted to the lock-in transition). Therefore, we conclude the following (see also Table V):

$E44$:	(mainly) Na(3) translation along **b**	antisymmetric	(B_g)
$E40$:	(mainly) Na(3) translation along **a**	antisymmetric	(A_g)
$E34$:	(mainly) CO_3 translation along **a**	antisymmetric	(A_g)
$E28$:	(mainly) CO_3 translation along **b**	antisymmetric	(B_g)

We are left with the modes $E46$, $E19$, $E16$, and $E10$. These modes are all rather weak. Because they are (except $E16$) not observable above 200 K, the assignment is even more difficult. Nevertheless, we would like to present here a few considerations. If we compare the two translational modes of Na(3) and CO_3 along **c**, which are antisymmetric, we expect their frequencies to be smaller than those of the corresponding modes along **a** or **b**. This

because of the smaller Na-O distances in the **a**, **b** plane, compared to the Na-Na or Na-C distances along **c** (de Wolff and Tuinstra[14]). The libration around **c** has a moment of inertia, which is approximately twice as big as that of the librations around **a** or **b**, resulting in a lower frequency. On the other hand, due to the stronger bonds in the **a**, **b** plane, the frequency is expected to be higher. Therefore, we suggest the following (see also Table V):

$E16$:	CO_3 libration around **c**	symmetric	(B_g)
$E19$:	(mainly) Na(3) translation along **c**	antisymmetric	(A_g)
$E10$:	(mainly) CO_3 translation along **c**	antisymmetric	(A_g)

The fact that the cluster (even above the lock-in transition) of three modes $E46$ to $E50$ is not assigned to a normal mode of the β-phase structure will be explained in the section concerning the lock-in transition.

2. The FIR spectrum

When we look at the FIR reflection spectrum (Fig. 4), the first striking feature is the resemblance to the Raman external mode spectrum. The FIR, however, has lines up

to 350 cm^{-1} and the line form is much broader.

The selection rules allow 15 IR active external modes in the β phase. Nine of these 15 modes correspond to the nine Raman active modes, where symmetric is replaced by antisymmetric, and conversely. The remaining six modes are numbers 18, 19, 22, 25, 26, and 27 in Table V. Those IR active modes in the β phase, which are inactive in the α phase are again expected to be weak in the monoclinic phase. These are all modes which are antisymmetric. The remaining nine strong modes are numbers 16, 17, 18,

and 20 up to 25 in Table V. The three acoustic modes, which are not IR active, are among these. Therefore, we expect six strong and six weak lines. The modes in which only the $Na(I)$ ions move will have relatively high frequencies with respect to the other ones and can thus be regarded as normal modes, because the $Na(I)$ ions are in the center of an octahedron of oxygen atoms, with small Na-O distances compared to the $Na(3)$-CO_3 distances.[14] Therefore, we suggest that the three strong modes observed above 200 cm^{-1} correspond to the three $Na(I)$ modes which are symmetric. Owing to the high frequencies of these modes, we can expect to see $k = nq$ (with $n \neq 0$) modes in the Raman spectrum, because they will not be obscured by $n = 0$ Raman lines. The three $n \neq 0$ Raman components at about 230 cm^{-1} correspond to the lowest one of the three high-frequency FIR modes (see the section on the lock-in transition). The two highest FIR modes have no component in the Raman spectrum. This can be explained by the fact that the 230-cm^{-1} mode is b-polarized and therefore couples to the modulation, while due to screening of the O atoms the $\partial \vec{\alpha} / \partial Q$ stays small for the other two modes, resulting in a low Raman activity at $k = nq \neq 0$. The remaining three modes are symmetric $Na(3)$-CO_3 translations parallel to a, b, and c. These modes can be assigned to the 100-, 170-, and 200-cm^{-1} lines. The c-polarized mode is probably the lowest lying because of the greater inter-ion distances. The remainder of the spectrum is difficult to interpret without more information. On the other hand, it might be possible that the 230-cm^{-1} mode is the b-polarized $Na(3)$-CO_3 mode, which is expected to appear resolved in the Raman spectrum, whereas the $Na(I)$ modes due to the screening mentioned above should give rise to less-resolved weak Raman lines.

E. The lock-in transition

The question of whether or not Na_2CO_3 undergoes a lock-in transition has attracted the attention of several investigators. The first evidence for a lock-in transition has been obtained by de Pater and Helmholdt by neutron diffraction on a single crystal first, and in a powder experiment later.[9] The commensurate value of the wave vector was found to be $q = \frac{1}{6}a^* + \frac{1}{3}c^*$, the space group $P2/a$, and the transition temperature about 130 K.

Subsequent x-ray diffraction however, revealed no lock-in transition[23] and the same negative result was found in experiments on specific heat and on the dielectric constant.[24] Even the Raman experiments done by Maciel and Ryan[8] showed no particular features in the neighborhood of the lock-in transition.

The presence or absence of a lock-in phase transition in different crystals of the same compound is a well-known phenomenon. Often these discrepancies between different samples are ascribed to the presence of defects or impurities for which incommensurate crystal phases are more sensitive than commensurate ones. In some cases, the impurities are claimed to be responsible for the absence of the transition;[25] in other cases they would be the cause of the presence of a commensurate phase.[26] In any case, these phenomena are still badly understood. The distinc-

tion between incommensurate and commensurate phases has little meaning in the limit of very large unit cells. In our case, however, the distinction between the twelvefold superstructure and the incommensurate phase appears very clearly in the Raman spectra. Looking at Fig. 3, we see below $T_c \approx 130$ K many modes which do not appear above this temperature. In fact, looking at the spectra, we see broad lines above 130 K, which resolve into rather sharp lines below this temperature. This effect is somewhat obscured by the broadening of the lines with increasing temperature. The striking feature is that, on lowering the temperature, almost all lines start at 130 K, and that indicates a phase transition. Furthermore, above this temperature the structure superimposed on the broad lines is not the same at every temperature; this means that above the transition the structure changes rapidly with temperature, and this is consistent with the presence of a temperature-dependent incommensurate modulation. The explanation for the resolving of many lines in the commensurate phase is the following. The low-temperature commensurate phase is modulated, the modulation giving rise to a fairly large number of inequivalent atomic positions within the unit cell of the superstructure, lattice periodicity ensuring sharpness in the Raman lines.

In the incommensurate phase, above the transition temperature T_c, the crystal consists of commensurate regions (precursors of the lock-in structure), but the incommensurability of the modulation wave imposes the presence of so-called discommensurations. From the point of view of the modulation wave, the whole is realized by a squared-like wave involving a fairly large number of higher harmonics. One can describe the same behavior using instead of higher harmonics the low-temperature modulation wave together with a position-dependent phase. In that case, the commensurate regions are characterized by a constant phase value, whereas the regions of discommensurations show a very rapid variation of the phase. This has two consequences for the Raman lines in the incommensurate regime. First of all, the presence of higher harmonics increases the intensity of the $k = nq$ modes for higher n values. Note, however, that even at room temperature, and thus far away from the lock-in transition temperature T_c, the modulation wave is already non-sinusoidal.[27] Second the discommensuration regions produce a broadening of the lines with respect to the corresponding ones in the commensurate phase. A consequence of the presence of higher harmonics is the increase of the intensity of the $k = nq$ modes (for higher n) in, e.g., the Raman spectrum. In Fig. 7 a schematic plot is shown for the Raman line form in both incommensurate and commensurate phases. We see that due to the incommensurate value of the wave vector, the line form is very broad, with a structure superimposed, depending on the value of q and the intensity of the various higher-order satellites. In the neighborhood of the lock-in transition the wave vector slowly drops to its commensurate value, when the temperature is lowered towards T_c, starting at approximately 200 K (de Pater and Helmholdt[9]). The change in the value of q causes the structure in the Raman line to change considerably because the change in the frequency shift of a line at $k = nq$ is approximately n

times the shift of the corresponding $k=q$ component. Moreover, instability of the value of q near the lock-in transition causes the structure in the line form to be less well defined.

Another way of looking at the line form in the neighborhood of the lock in is to consider a superstructure approximation, describing the structure as a (twelvefold) superstructure with small deviations:

$$q = (1/6 - \delta_1)a^* + (1/3 - \delta_3)c^* ,$$

where $\delta_1 \ll 1/6$ and $\delta_3 \ll 1/3$. Now the line form will be that of the twelvefold superstructure perturbed, however, by additional modes due to the deviations. Again, higher harmonics are needed to explain the strength of the additional modes, and the pronounced temperature dependence of the lines observed. In the commensurate case, apart from decrease of thermal broadening, the spectrum is much less sensitive to temperature changes. It is mainly the intensity of the resolved peaks which changes with temperature; this is an effect due to variation in the modulation waveform.

The activity of the modes at $k = nq$, both in the incommensurate and in the commensurate phase, can be obtained by means of the super-space-group symmetry of the structure. In the present paper, this has already been done (for the incommensurate phase) up to the terms involving $n = \pm 1$. In the superstructure case, because of the large (twelve-fold) supercell, the enormous matrices needed while using ordinary space groups, reduce (thanks to the super-space group) easily to twice the size of the matrices needed in the normal phase. The results of the analysis are given in Table VI. We see that every Raman active (gerade) mode for $n=0$ splits into seven Raman and five IR active components in the δ phase. The opposite (i.e., five Raman and seven IR components) holds for the IR (ungerade) $n=0$ modes. The distinction between the A and B symmetries will not be of much use because of the lack of single crystals. The expected clusters of seven or five modes represent an upper limit. This can be seen in Fig. 7; the splitting of the components depends on the dispersion of the nonperturbed branch and on the splitting of the modes at $k = nq$, the latter being due to the coupling with the modulation.

At this point a distinction between external and internal modes is relevant again. The consistency between the approach described above and the one in the WTB model is as follows. In the incommensurate phase, for a sinusoidal modulation, the splitting will be mainly present at $k = \pm q$, the higher-order gaps decreasing very fast in magnitude.[16,17] In the case of the ν_1 mode, for example, the zeroth-order A_g mode has a B_g first-order mode (at $k = \pm q$). The difference in intensity due to the difference in perturbation, is compensated by the relatively large number of ions perturbed by the modulation as compared to those which are not affected. This result is comparable with the two singularities with equal intensity as predicted by WTB model.

If, on the other hand, the modulation waveform is rather squarelike, higher harmonics of $k = \pm q$ will be present and therefore the dispersion curve will show first-order gaps at $k = nq$ ($n = \pm 1, \pm 2, \pm 3, \ldots$) too. For a flat dispersion this will result in two peaks, one corresponding to the zeroth-order frequency, the other to the frequency which is perturbed in first order, again assuming that the higher-order perturbations are negligible. As a result, the intensity of the line corresponding to the unperturbed frequency will be stronger than the other one.

In the region where the modulation has a waveform between a sinusoidal and a square wave, the two singularities are expected to be broader and less well resolved. In the commensurate phase the modulation can be described by a waveform resembling to a great extent a square wave.

TABLE VI. Super-space-group analysis of the modes (at $k = nq$) which are equivalent with $k = 0$ in the β, γ, and δ phases. In the γ phase one has a pair consisting of a *gerade* and an *ungerade* mode for each value of $|n| \neq 0$.

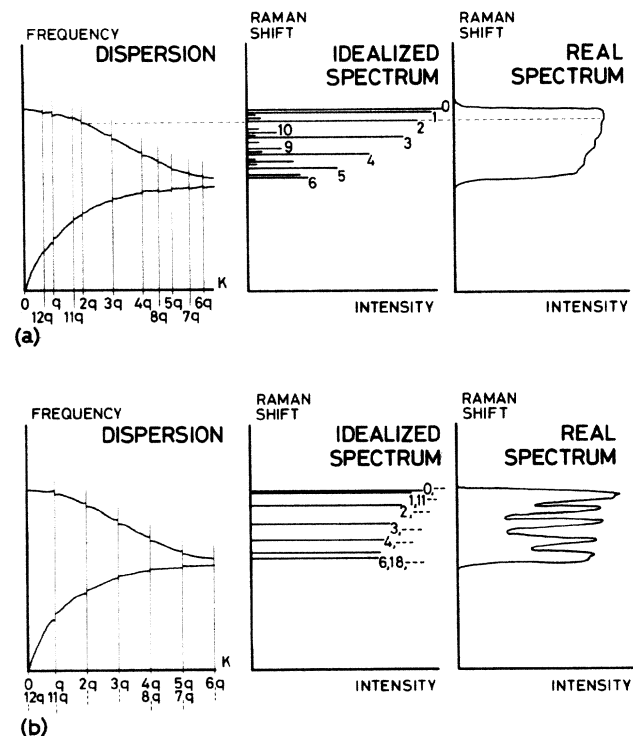| β phase	γ phase $n = 0, \pm 1, \pm 2, \pm 3, \ldots$	δ phase
$A_g \rightarrow$	$A_g + B_u^{A_u} + B_g^{A_g} + B_u^{A_u} + \cdots \rightarrow$	$4A_g + 3B_g + 3A_u + 2B_u$
$B_g \rightarrow$	$B_g + B_u^{A_g} + B_u^{A_u} + B_g^{A_g} + \cdots \rightarrow$	$3A_g + 4B_g + 2A_u + 3B_u$
$A_u \rightarrow$	$A_u + B_u^{A_g} + B_u^{A_u} + B_g^{A_g} + \cdots \rightarrow$	$3A_g + 2B_g + 4A_u + 3B_u$
$B_u \rightarrow$	$B_u + B_g^{A_u} + B_u^{A_g} + B_g^{A_u} + \cdots \rightarrow$	$2A_g + 3B_g + 3A_u + 4B_u$

FIG. 7. Expected Raman line form (a) in the incommensurate phase near the lock-in transition and (b) in the commensurate phase. In the incommensurate phase not all lines are drawn for clarity. The relevant ones occur when the corresponding gap is significant (see broken lines). The intensities are arbitrarily chosen.

TABLE VII. The Raman lines belonging to the different clusters in the δ phase. The choice of the components is sometimes disputable. The identifiers En can be found in Fig. 2 and partly in Fig. 3. The maximum number of components (see also Table VI) is given too.

Cluster	Components	Maximum number
$C48$	$E\,50, E\,48, E\,46$	5
$C44$	$E\,45, E\,44, E\,42, E\,41$	7
$C40$	$E40$, perhaps $E38$	7
$C34$	$E34$, perhaps $E33$	7
$C28$	$E\,28, E\,26, E\,25, E\,24$	7
$C19$	$E\,20, E\,19$	7
$C16$	$E\,18, E\,16, E\,14, E\,12$	7
$C10$	$E10$	7
$C8$	$E\,8, E\,6, E\,4$	7

Hence, there are relatively many ions at positions where $\eta = \eta_{max}$ and very few at $\eta = 0$. Again the different orders of perturbations between these lines will compensate the asymmetry in the lines.

In conclusion, the expected line form will depend largely on the modulation waveform as a function of temperature and on the form of the dispersion curves for the different branches. If we return our attention to the experimental results, we recognize, looking at the Raman spectrum, the different clusters resolved at the lowest temperature.

F. The external modes in the δ phase

In this section we will explain how the different line forms of the clusters observed in the spectra of the δ phase can be understood in terms of modes coupling to the modulation, using the results of the assignments in the γ phase. The Raman lines belonging to the different clusters (Cn) are given in Table VII.

Those modes for which the movements of the ions are (partly) along b, will couple strongly to the modulation, giving rise to a large splitting in several components. This is the case for the clusters $C44$, $C28$, and $C16$. The opposite holds for the modes with no (or small) motions along b; they will show no or small splitting. This holds for the clusters $C40$, $C34$, $C19$ (although too weak), and $C10$.

Beside the splitting of the clusters, additional modes can be expected due to ($k=0$) IR active modes. Cluster $C48$ provides the clearest example of such lines; where due to the absence of a (strong) $n=0$ line, the components are quite well resolved, even above the lock-in transition.

Cluster $C44$ can also contain $k=n\mathbf{q}$ contributions due to a strong FIR line at the same frequency. Component $E18$ of cluster $C16$ clearly grows in intensity with decreasing temperature, starting at T_c. In the FIR a small though clear mode at 100 cm^{-1}, visible up to 130 K is seen. These modes are probably related. Finally, the Raman lines $E38$ and $E36$ are isolated and have corresponding lines in the FIR spectrum. Hence, one expects the former to be $n \neq 0$ components of the FIR lines. The same holds for $E32$ and perhaps $E30$. It is, however, difficult to assign these lines to normal modes.

The FIR spectrum gives no further clear information

on the lock-in transition, probably because of the broader peaks as compared to the Raman lines. Only a decreasing line width is observed by lowering the temperature.

V. CONCLUSION

We have measured the complete Raman spectra of Na_2CO_3 in the monoclinic (β), the incommensurate (γ), and the commensurate lock-in (δ) phases. The far-infrared spectra have been obtained in the γ and in the δ phases. The different lines have been assigned and interpreted by using symmetry as well as phenomenological arguments. Most of the lines found have been assigned to the different phonon modes of the β phase.

As the selection rules (obtained by using the super-space group of γ-Na_2CO_3) predict, additional modes are active in the incommensurate phase. A few of these modes have been seen and interpreted in both the Raman and IR spectra. The additional modes (lying at $k=n\mathbf{q}$ for $n \neq 0$ in the β phase) often differ not much in frequency from the corresponding modes at $k=0$. This and the fact that their optical activity is mostly rather small, causes the difficulty in observing these modes in the different spectra. We nevertheless have found additional modes which were resolved because of three different reasons:

(1) The Raman lines $E50$, $E48$, $E46$, $E38$, $E36$, $E32$, $E18$, and perhaps $E30$ are interpreted as corresponding to $n \neq 0$ components of IR active modes at $k=0$. The absence of the relatively strong $k=0$ component and the fact that these additional modes are not obscured by other (strong) Raman active modes makes them observable.

(2) Those branches which are mainly b polarized, will be most sensitive to the modulation. Therefore the gaps at $k=n\mathbf{q}$ will be the largest for these branches. This is observed in the Raman spectra of the commensurate phase, where the b polarized modes consist of clusters which have more components resolved than modes which are mainly a or c polarized.

(3) The soft mode belonging to the phase transition to the incommensurate phase has wave vector $k=\pm\mathbf{q}$ and is a resolved "additional mode" due to its temperature-dependent frequency and intensity near the phase transition.

For the internal modes (vibrations of the CO$_3$-ion constituents), the line shape is better described by a frequency distribution, which is determined by the modulation amplitude in the vicinity of the different CO$_3$ ions. This frequency distribution has two singularities at the frequencies corresponding to a maximal- and minimal-modulation displacement. The intensities of the corresponding peaks in the spectra depend mainly on the number of higher harmonics involved in the modulation waveform. The higher the frequency of an internal mode, the flatter is its dispersion and therefore the better this description in terms of a frequency distribution holds.

Two soft modes have been found in the Raman spectra. One is identified as belonging to the hexagonal-to-monoclinic phase transition; the other one belongs to the monoclinic-to-incommensurate phase transition; this in contrast to results of earlier measurements of Maciel and Ryan.[8] We conclude that of the two soft mode components, corresponding to the hexagonal-to-monoclinic phase transition, the symmetric libration around b corresponds to the Raman line $E8$, while the libration around a stays low in frequency ($\omega < 20$ cm^{-1}) for temperatures below the phase-transition temperature. The symmetric librational mode around a at k$= \pm$q, which becomes soft together with the b-polarized acoustic mode at k$= \pm$q at the monoclinic-to-incommensurate phase transition, is observed as $E2$ in the Raman spectra.

Finally, we have found clear evidence for a third phase transition to a lock-in (δ) phase at 130 K, which was seen only once before (de Pater and Helmholdt[9]). The effect on the line shape on going from an incommensurate-to-commensurate phase has been discussed and appears to fit well with the experimental results. In short (see Fig. 7), the line form in the incommensurate phase is broad and shows a structure superimposed, which is not well reproducible for different temperatures. Owing to the increasing number of higher harmonics in the modulation waveform on approaching the lock-in transition, the intensities of the modes at k$=n$q for higher values of n increase. This and the incommensurate value of the modulation wave vector gives rise to a dense cluster of lines in the spectra. The strong temperature dependence of q in the neighborhood of the lock-in transition makes the structure of these clusters also strongly temperature dependent. In the lock-in phase, on the other hand, the commensurate value of q gives rise to a discrete number of lines for each phonon branch, resulting in clusters of fairly sharp lines. The number of lines observed is determined by the symmetry of the different cluster components and the effects of the modulation on the mode involved.

ACKNOWLEDGMENTS

*Present address: Department of Physics, University of California, Berkeley, CA 94720.

†Present address: Hochfeld-Magnetlabor, Max-Planck-Institut für Festkörperforschung, Boîte Postale 166X, F-38042 Grenoble Cédex, France.

[1]H. Meekes, K. Hanssen, A. Janner, T. Janssen, P. Wyder, and Th. Rasing, Ferroelectrics 53, 285 (1984).

[2]P. M. de Wolff, Acta Crystallogr. Sect. A 33, 493 (1977).

[3]A. Janner and T. Janssen, Phys. Rev. B 15, 643 (1977).

[4]A. Janner and T. Janssen, Acta Crystallogr. Sect. A 36, 399 (1980); 36, 408 (1980).

[5]W. Hayes and R. Loudon, Scattering of Light by Crystals (Wiley, New York, 1978).

[6]Th. Rasing, P. Wyder, A. Janner, and T. Janssen, Phys. Rev. B 25, 7504 (1982).

[7]M. H. Brooker and J. B. Bates, J. Chem. Phys. 54, 4788 (1971).

[8]A. Maciel and J. F. Ryan, J. Phys. C 14, L509 (1981).

[9]C. J. de Pater and R. B. Helmholdt, Phys. Rev. B 19, 5735 (1979).

[10]W. van Aalst, J. den Hollander, W. J. A. M. Peterse, and P. M. de Wolff, Acta Crystallogr. Sect. B 32, 47 (1976).

[11]F. Tuinstra (private communication).

[12]K. E. H. M. Hanssen, Doctoraalscriptie, Katholieke Universiteit Nijmegen (1983), p. 65.

[13]M. H. Brooker and J. B. Bates, Spectrochim. Acta, Part A 30, 2211 (1974).

[14]P. M. de Wolff and F. Tuinstra, in Incommensurate Phases in Dielectrics, edited by R. Blinc and A. P. Levanyuk (North-Holland, Amsterdam, 1986), Vol. 2, p. 253.

[15]T. Janssen, J. Phys. C 12, 5381 (1979).

[16]T. Janssen and C. de Lange, J. Phys. (Paris) Colloq. 42, C6-737 (1981).

[17]T. Janssen, in Incommensurate Phases in Dielectrics, edited by R. Blinc and A. P. Levanyuk (North-Holland, Amsterdam, in press), Vol. 1.

[18]G. Herzberg, Molecular Spectra and Molecular Structure (Van Nostrand, New York, 1954), p. 178.

[19]R. Blinc, S. Juznic, V. Rutar, J. Seliger, and S. Zumer, Phys. Rev. Lett. 44, 609 (1980).

[20]A. Maciel, J. F. Ryan and P. J. Walker, J. Phys. C 14, 1611 (1981).

[21]P. C. B. Crooijmans (unpublished).

[22]M. Wada, A. Sawada, Y. Ishibashi, and Y. Takagi, J. Phys. Soc. Jpn. **42**, 1229 (1977).

[23]P. C. B. Crooijmans, G. H. Kolkman, and F. Tuinstra, Abstr. Eighth European Crystallographic Meeting, Liège, 1983, p. 243 (unpublished).

[24]M. Midorikawa, K. Tsunoda, and Y. Ishibashi, J. Phys. Soc. Jpn. **49**, 242 (1980).

[25]R. P. A. R. van Kleef, Th. Rasing, J. H. M. Stoelinga, and P. Wyder, Solid State Commun. **39**, 433 (1981).

[26]K. Hamano, T. Hishinuma, and K. Ema, J. Phys. Soc. Jpn. **50**, 2666 (1981).

[27]A. Hogervorst, W. J. A. M. Peterse, and P. M. de Wolff, in *Modulated Structures,* AIP Conf. Proc. No. 53, edited by J. M. Cowley, J. B. Cohen, M. B. Salamon, and B. J. Wuensch (AIP, New York, 1979), p. 217.